Tuning the electronic properties of monolayer and bilayer transition metal dichalcogenide compounds under direct out-of-plane compression

Ángel Morales-García [a*], Elena del Corro [b*], Martin Kalbac [b], Petr Nachtigall [a], Otakar Frank [b]

[a] *Department of Physical and Macromolecular Chemistry, Faculty of Science, Charles University in Prague, Hlavova 2030, 128 43 Prague 2, Czech Republic*

[b] *J. Heyrovsky Institute of Physical Chemistry of the AS CR, v.v.i, Dolejskova 2155/3, 182 23 Prague 8, Czech Republic*

*e-mail: a.moralesg@natur.cuni.cz , edelcorro@quim.ucm.es

Abstract

The band-gap modulation of atomically thin semiconductor transition metal dichalcogenides (MX_2; *M*=Mo or W, *X*=S or Se) under direct out-of-plane compression is systematically studied by means of the density functional theory formalism. This stress regime significantly reduces the pressure threshold at which the semimetal state is achieved (2.7-3.1 and 2.0-3.5 GPa for mono- and bilayer systems, respectively). Structural, electronic and bonding properties are investigated for a better understanding of the electronic transitions achieved with compression. A notable relationship with the formal ionic radius (M^{4+} and X^{2-}) is found out. On one hand, the monolayer systems with the smallest transition metal radius ($Mo^{4+} < W^{4+}$) reach the semimetal state at the lower stress, on the other hand, for bilayer specimens the transition to semimetal is observed earlier for compounds with the smallest chalcogenide radius ($S^{2-} < Se^{2-}$). Moreover, the appearance of non-covalent interaction (NCI) domains in the semimetal state confirms that the out-of-plane compression promotes the interaction between sulfur atoms in the single layered systems and reduces the interlayer space in bilayer configurations. Our predictions, supported by experimental evidences in the case of monolayered MoS2, open new alternatives for tuning the electronic properties of transition metal dichalcogenides under direct out-of-plane compression.

Introduction

The field of 2D semiconductor transition metal dichalcogenides (TMDs) is being widely investigated due to their outstanding electronic properties, ideal for optoelectronic devices [1-2]. The direct band-gap characteristic of monolayered (1L) TMDs evolves into an indirect one when the sample thickness increases. Tuning the band-gap of TMDs (MX_2, *M*= Mo, W and *X*= S, Se) with the aid of strain constitutes an important strategy to enhance the performance of electronic devices [3]. Recently, several works have reported the strain engineering on monolayered MoS_2, WS_2, $MoSe_2$ and WSe_2 systems from an experimental and a theoretical point of view [4 , 5 , 6 , 7 , 8 , 9 , 10] showing the crucial importance that the strain regime and direction may have on the absolute band-gap energy modulation with progressive deformation. Additionally, the strain-tuning gains another degree of freedom in TMD systems with two or more layers through the modification of the interlayer coupling [11,12,13]. The band-gap modulation, therefore, depends mainly on two factors: (i) the size of the system (the strain range required to alter the band-gap is different in monolayer, bilayer (2L) or bulk systems); and (ii) the direction and regime of strain (*i.e.* uniaxial, biaxial or hydrostatic) [9 ,14].

Concerning high pressure, several experimental studies coupled with computational predictions have been carried out to investigate multilayered MX_2 systems under hydrostatic conditions [11,15,16,17]. All these high pressure experiments are performed using diamond anvil cell (DAC) devices. A semiconductor to semimetal transition is commonly observed for all compounds at pressure values ranging from 19 to 40 GPa depending on the composition. Nayak *et al.* [11] reported the study of multilayered MoS_2, where a structural lattice distortion (within the same crystal structure) is observed along with an electronic transition from semiconductor to semimetal at 19 GPa, with the theoretical prediction of such transition being approximately 24 GPa. The metallization arises when the interlayer space is reduced leading to S-S interactions and to the overlapping of the valence (Γ point in the Brillouin zone) and the conduction (between K and Γ points) bands. The same authors [16] investigated multilayered WS_2, revealing that the band-gap closure is modulated by the increase of the interlayer S-S interactions at pressures above 22 GPa (similar pressure is predicted using first-principles calculations). Other study, published by Zhao *et al.* [15], analyzed the behavior of multilayered $MoSe_2$. They also

found that the pressure induced the metallization, analogously to that observed for MoS_2, at 40 GPa, in good agreement with the theoretical predictions (41 GPa). Previously to these studies, Liu *et al.* [17] reported the metallization of multilayered WSe_2 at 38 GPa, slightly above theoretical predictions (35 GPa), with this electronic change accompanied by an isostructural phase transition. By comparing all these previous studies, it is noted that the sulfide compounds (MS_2) undergo the transition to a metal state at substantially lower pressures than selenide ones (MSe_2).

Among all monolayered TMDs compounds, 1L-MoS_2 has been investigated under different strain regimes. Concerning high pressure studies, we find that the effect of hydrostatic pressure on the TMDs' electronic structure has been analyzed: first the direct band-gap energy increases [14] while the indirect one is reduced, leading to a direct to indirect band-gap transition at 23 GPa; then the semiconducting to semimetal transition is theoretically predicted to happen at ~68 GPa. More recently, it has been demonstrated that the application of small out-of-plane axial compression can be used for strain engineering of the electronic structure of 1L-MoS_2 [9]. This experimental study combined with first-principles calculations reports that the transition from direct to indirect band-gap semiconductor takes place at only 0.5 GPa, followed by a transition to the semimetal state at values of compression below 3 GPa. It must be noted that the stress along the out-of-plane direction required to metallize the 1L-MoS_2 is twenty times lower than the needed hydrostatic compression. To the best of our knowledge, there are no high pressure studies of other monolayer TMDs under this non-hydrostatic regime and most of the existing literature is devoted to the analysis of the effects of biaxial or uniaxial in-plane strain. Wang *et al.* [18] studied the strain dependence of the light emission and lattice vibration of CVD-grown monolayer WS_2 proving the tuning of different optical transition energies by applying uniaxial in-plane strain, complemented with DFT calculations. They concluded that this tunable optical property is attributed to the strain-induced direct to indirect band-gap transition. Ghosh *et al.* [19] investigated the equibiaxial strain effect on the electronic and optical properties of monolayer $MoSe_2$ finding out that the transition indirect-to-direct band-gap semiconductor is directly related with the reduction of the monolayer thickness. It is noted that the metallization is not observed under in-plane uniaxial and equibiaxial strain regimes [18-

[19]. The electronic properties have been also investigated recently for monolayer WSe_2 under biaxial tensile and compressive strain using first-principles calculations [20]. The authors found out that the monolayer WSe_2 retains the direct band-gap state under tension and such band-gap continuously decreases with increasing strain; and strains larger than 13% are required to reach the semimetal state. To date, the out-of-plane compression [9] is proved to be the most effective regime to achieve the semimetal state, leading to promising future developments in strain-modulated advanced devices.

Direct out-of-plane compressive regime is used here to theoretically investigate the structural, electronic and chemical properties of mono- and bilayer TMDs. Our previous theoretical predictions of monolayer MoS_2 [9] are, in the present work, extended to other specimens of the family ($MoSe_2$, WSe_2 and WS_2); we show a systematic analysis of the structural properties and their relationship with the modulation of the band-gap. Additionally, the chemical properties are evaluated using non-covalent interaction (NCI) index to analyze the formation of new weak interactions induced by the direct out-of-plane compressive regime.

Methodology

First-principles calculations are performed on unstrained (pristine) and strained mono- and bilayer TMDs compounds applying direct out-of-plane compression. To this propose, the density functional theory (DFT) formalism [21, 22] is used as implemented in the Vienna *Ab initio* Simulation Package (VASP) code [23, 24]. The generalized gradient approximation of Perdew, Burke and Ernzerhof (PBE) [25] is selected to solve the Kohn-Sham equations keeping the consistency with recent studies [11, 9]. Projector augmented wave (PAW) potentials [26] are used to describe the electron-ionic core interaction and Brillouin zone integrals are approximated using Monkhorst and Pack method [27]. The energies are converged with respect the *k*-point density 10x10x1 for both mono- and bilayer systems and the plane-wave cutoff of 560 and 340 eV (MS_2 and MSe_2 systems, respectively) is used to ensure convergence of the total energy within 10^{-5} eV and the geometry optimization stops when the force on each ion is less than 0.01 eV/Å. The optimization of lattice parameters is calculated using the bulk unit cell of MoS_2, WS_2,

$MoSe_2$ and WSe_2. A vacuum of 10 Å to avoid the interaction between periodic slabs images along *z*-direction.

To mimic the experimental conditions of direct out-of-plane compression on monolayer compounds [9], the *X*-*X* distance decreases along the *z*-direction and *M* atoms are allowed to relax, keeping the *a* and *c* lattice parameters frozen during the process. The stress, which acts on the cell, is obtained in the three directions *z* and *x*(=*y*). The in-plane/out-of-plane stress ratio is in good agreement with previous experimental evidences using moissanite anvil cells [28]. Different constraints are used in the case of bilayer systems where the monolayer units are moved reducing the van der Waals space between them, the external chalcogenide atoms are fixed whereas the rest of the atoms located between them are relaxed, keeping the lattice parameter constant as in the monolayer case. The out-of-plane stress values are multiplied by a correction factor considering the relationship between the unit cell top-bottom surface and the real section occupied by the atoms in the unit cell. Stress values coincided with those calculated as the energy cost over the cell volume taking the *X*-*X* distance as *c* parameter in the monolayer systems (more details over the model was recently published in [9]).

Results and discussion

Monolayered TMDs

The structural and electronic properties of 1L TMDs in their pristine state are reported in Table 1. These results are calculated using the PBE exchange-correlation functional; it is well-known that the structural properties (*i. e.* lattice parameter) are overestimated whereas the electronic ones (*i. e.* band-gap) are underestimated with respect to the experimental data when using the generalized gradient approximation (GGA) functional as PBE. The deviations associated with the lattice parameter are below 1 % (0.7 and 0.5 % for MoS_2 and $MoSe_2$, respectively, and below 0.8 % for WS_2 and WSe_2)[29]. On the other hand, the band-gap is clearly underestimated, with 1.6, 6.4, 5.1 and 4.2 % deviations for MoS_2, $MoSe_2$, WS_2 and WSe_2, respectively[9, 30, 31]. The deviation of the band-gap can be solved using hybrid functionals, which are widely used to

investigate the electronic properties of semiconductor compounds, but the required computational time is high. For this reason, previous studies reported the modulation of the band-gap of TMDs compounds under different pressure regimes [9,11] using the PBE functional, justifying our choice, which - as we will show next - gives reasonable results, consistent with those published. In addition, the errors generated by PBE functional do absolutely not affect the conclusions of the work.

Table 1. Structural properties of monolayer MX_2 compounds: lattice parameter, *a,* bond distances, *d*(*M*-*X*), *d*(*X*-*X*), and bond angle, θ(*X*-*M*-*X*). The band-gap, E_g, corresponds to the direct band-gap (K–K) along the Brillouin zone. Our results are compared with experimental data available in the literature.

Compound		***a*, Å**	***d*(*M*-*X*), Å**	***d*(*X*-*X*), Å**	**θ(*X*-*M*-*X*),^{0}**	**E_g, eV**
MoS_2	PBE	3.183	2.405	3.151	81.791	1.82
	Exp	3.160 [29]				1.85 [9]
WS_2	PBE	3.182	2.416	3.139	81.013	1.84
	Exp	3.155 [29]				1.94 [30]
$MoSe_2$	PBE	3.315	2.541	3.341	82.222	1.47
	Exp	3.299 [29]				1.57 [31]
WSe_2	PBE	3.314	2.545	3.355	82.483	1.58
	exp	3.286 [29]				1.65 [31]

In the absence of pressure, the analysis of the band structures (black lines in Figures 1 a-d) clearly shows that the gap is governed by a direct transition with the highest and lowest energy level of the valence (VB) and the conductive (CB) bands, respectively, located in the *K* point of the Brillouin zone. This direct band-gap energy is slightly lower than the indirect band-gap, where the VB maxima (VBM) and the CB minima (CBM) are located in *Γ* and *K*, respectively. It must be pointed out that monolayered MS_2 systems present around 0.3 eV larger band-gaps than MSe_2 monolayers, showing an inverse correlation with the *X*–*M*–*X* bond angle, which is higher for MSe_2 compounds. In fact, *X*–*X* and *M*–*X* distances are also lower in MS_2 than in MSe_2, in accordance with the bond angles (*i. e.* small bond angles and distances correspond to larger band gaps, and vice versa). This structural-electronic analogy may be explained using the effective ionic radius described by Shannon-Prewitt [32]. The formal Se^{2-} and S^{2-} ionic radii are

198 and 184 pm, respectively. Thus, the monolayer with the largest chalcogenide ionic radius presents the smallest band-gap energy, due to the strong hybridization between *M* and *X* orbitals [33]. Other interesting issue is related with the transition metals, where MoX_2 monolayers show lower band-gap than WX_2 ones. This fact is related with the formal transition metal ionic radius: 59 and 89 pm for Mo^{4+} and W^{4+}, respectively. And, as we will discuss next, the transition metal ionic radius plays a significant role when the monolayer compounds are subdued to direct out-of-plane compression.

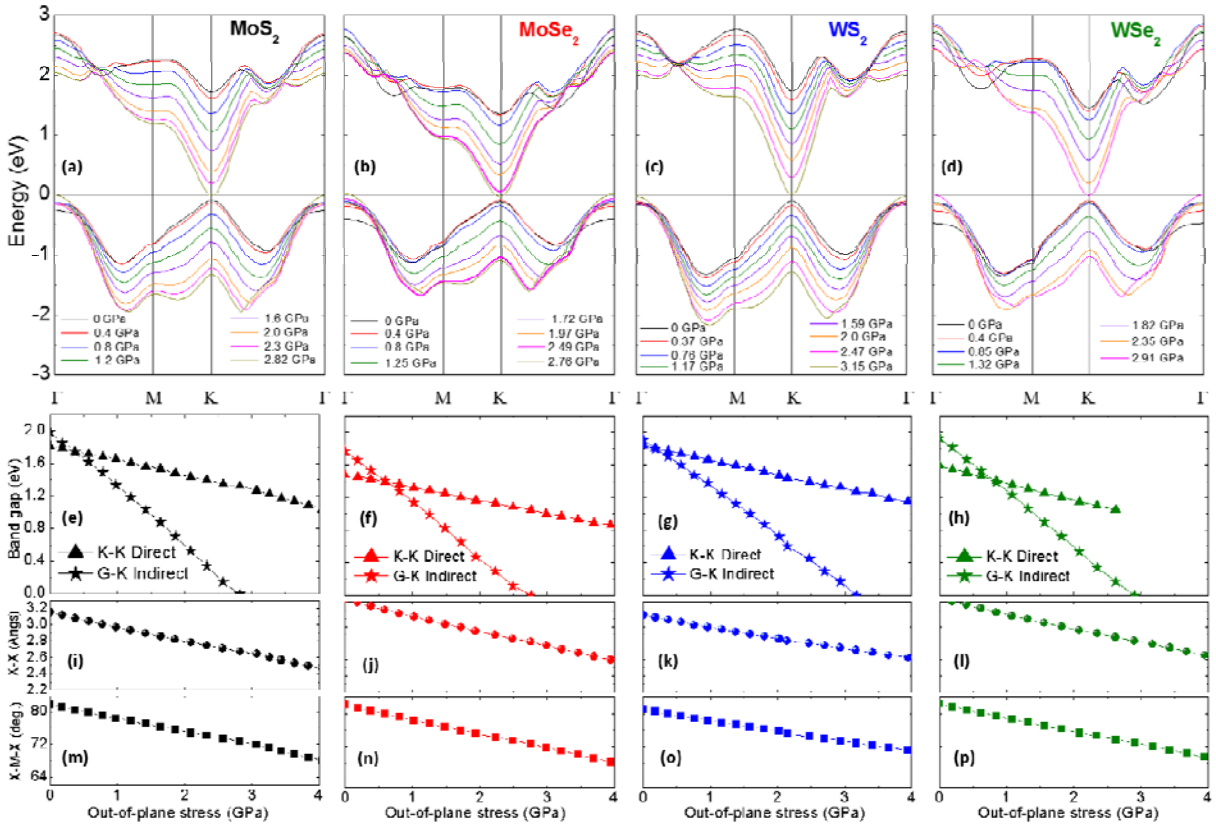

Figure 1. (a-d) Evolution of the VB and the CB under direct out-of-plane stress of 1L MX_2 monolayers (Fermi level is set to 0 eV). (e-h) Evolution of the direct (K-K) and the indirect (Γ-K) band-gaps and the structural parameters: *X*–*X* distance (i-l) and *X*–*M*–*X* bond angle (m-p).

The evolution of the direct and indirect band-gaps with compression is presented in Figures 1e-h. A direct-to-indirect semiconductor electronic transition takes place first, followed by the semiconductor-semimetal one (metallization process). This first electronic transition is achieved

at 0.17, 0.40, 0.62 and 0.81 GPa for WS_2, MoS_2, $MoSe_2$ and WSe_2, respectively (see inset in Table 2). Sulfides transform to an indirect semiconductor state before selenides, suggesting that the compounds formed by the chalcogenide with the smaller ionic radius (S^{2-} < Se^{2-}) requires lower compression to achieve the transition. For the particular case of monolayer MoS_2 compound, we found a good agreement between the experiments and the calculations [9] for the direct to indirect band-gap transition pressure.

The second electronic transition observed, the semimetallization, is achieved at 2.76, 2.82, 2.91 and 3.15 GPa for $MoSe_2$, MoS_2, WSe_2, and WS_2, respectively, as indicated in the inset Table in Figure 2. It is clear that monolayered MoX_2 compounds undergo the semimetallization (Figure 1 e-h) before than the WX_2 ones, with the transformation governed by the ionic metal radius, Mo^{4+} < W^{4+}. Hence, there is a clear difference in the tendency for the first and the second electronic transition, as shown in Figure 2 for clarity. While the direct to indirect semiconductor transition is governed by the chalcogenide radius, in the case of the metallization the transition order is determined by the metal ionic radius, as we explain next.

In Figures 1 i-p, we present the evolution of the structural parameters with the out-of-plane stress. These figures show the efficiency of such kind of compression in the reduction of the X-X perpendicular distance and the subsequent closure of the *X-M-X* angle. It is known that the electronic structure has the main contribution from d_{z^2} (out-of-plane), $d_{x^2-y^2}$ and d_{xy} (in-plane) orbitals of *M* atoms and *p* orbitals of *X* atoms [33]. It is noted that the VBM at *Γ* and the CBM at *K* are both dominated by d_{z^2} and the orbital contributing to the local minimum point of the lowest conduction band along *Γ* to *K* direction exhibits strong in-plane orbitals ($d_{x^2-y^2}$ and d_{xy}) character. Such orbital distribution is reflected in the strong correlation between the *X-M-X* angle closure rate and the metallization stress, as presented in Figure 3; note that the metallization is reached when the CB and the VB reach the Fermi level in the *K* and *Γ* points of the Brillouin zone, respectively.

The described phenomenon would also explain the quite different reported response of monolayer MoS_2 under out-of-plane and hydrostatic conditions [9, 14]. The decrease of the *X-M-*

X bond angle makes Mo *d* orbitals interact strongly with S *p* orbitals. This strong hybridization between the orbitals decreases the band-gap towards its closure.

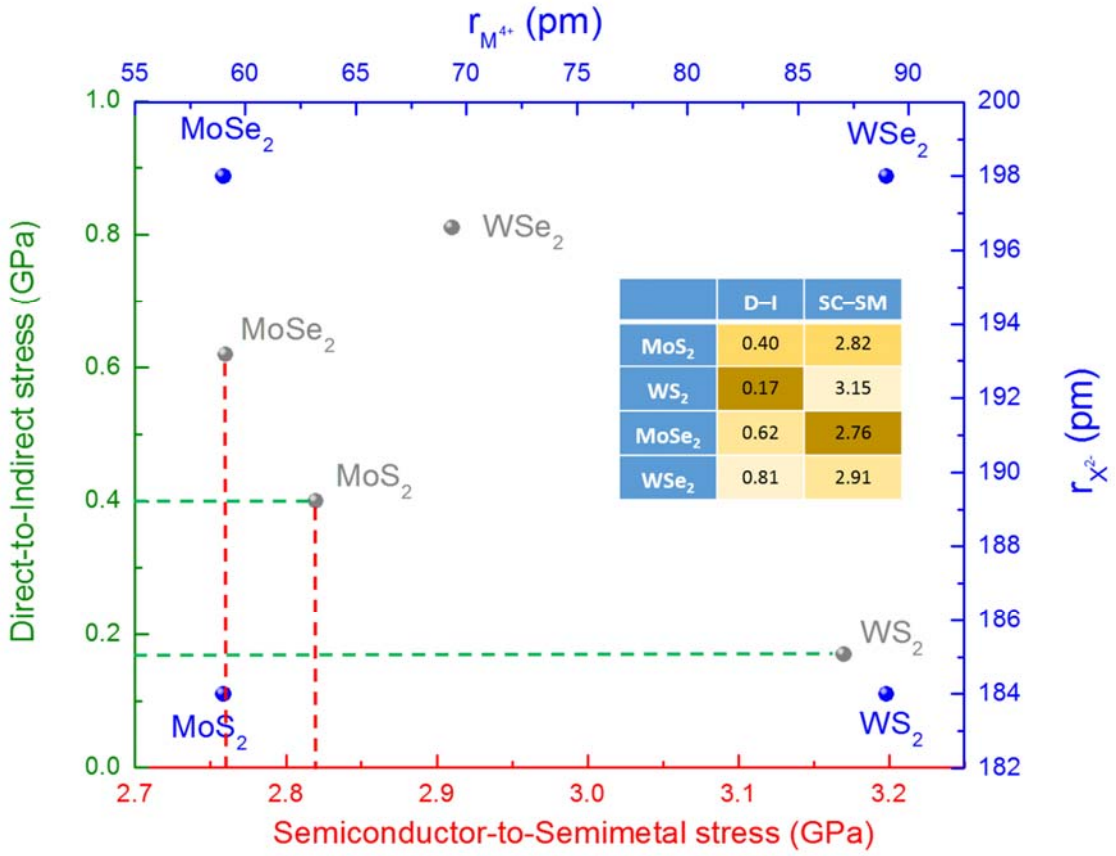

Figure 2. Blue, green and red axes correspond to atomic radii, direct-to-indirect and semiconductor-to-semimetal transition stresses, respectively. Blue spots correspond to the location of MX_2 compounds as a function of M^{4+} and X^{2-} radius and gray spots appear as the relation between the two electronic transitions. Red dashed lines indicate that 1L MoX_2 monolayer compounds require the smallest stress to reach the semimetal state whereas, green dashed line show that 1L MS_2 compounds undergo the transition to indirect band-gap SC at lower stresses than 1L MSe_2. The inset table shows the out-of-plane stresses at which the electronic transitions are observed. The color gradient correspond to the stress, the darkest color labels the lowest stress.

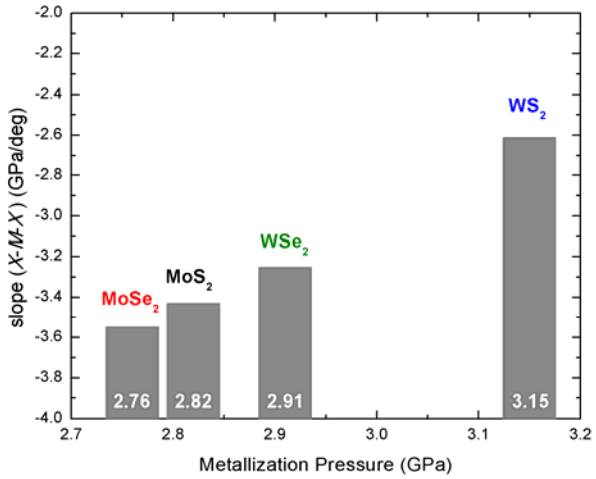

Figure 3. Relationship between the bond angle (*X-M-X*) closure rate and the metallization stress. The white values inside the gray bars are the semimetal pressures of monolayer systems (Figure 2 inset).

Bilayered TMDs

Bilayered TMDs compounds are also investigated under the direct out-of-plane compression. The electronic properties in the pristine state of semiconductor TMDs with more than one layer are governed by the indirect band-gap. As we discussed above (monolayered TMDs), the computational band-gaps are underestimated, with deviations of 0.6, 5.2, 1.6 and 3.2 % for bilayered MoS_2, $MoSe_2$, WS_2 and WSe_2, respectively (see Table 3 for the comparison between theory and experiment) [27, 34, 35, 36]. In Figures 4 a-d, the evolution of the VB and CB with out-of-plane compression are shown for 2L TMDs. In the pristine state (black lines), the VBM and the CBM are located in *Γ* and *K*, respectively, for sulfur compounds (MS_2); whereas the VBM and the CBM are located in *K* and between *K-Γ*, respectively, for the selenides (MSe_2). The semimetal state is achieved at 2.07, 2.38, 2.85 and 3.55 GPa for 2L MoS_2, WS_2, $MoSe_2$, WSe_2, respectively (Figure 4 e-h and Table 3). An intriguing behavior is observed when comparing the metallization stress of 1L and 2L systems: within 1L TMDs the metal state is achieved at lower stress by the MoX_2 compounds, whereas in the case of 2L specimens sulfides metalize before than selenides. Moreover, we observe that the bilayered sulfides metallize at lower pressure

than their monolayered counterpart; however, this behavior is opposite for selenide compounds.

Table 3. Theoretical and experimental indirect band-gap of 2L-TMDs (in eV) along with the values of metallization stress. Our results are compared with experimental data available in the literature.

Bilayer		MoS_2	WS_2	$MoSe_2$	WSe_2
Indirect band-gap (eV)	**Present work**	1.59	1.79	1.44	1.53
	experimental	1.60 [34]	1.82 [35]	1.52 [27]	1.58 [36]
Semiconductor-to-Semimetal (GPa)		2.07	2.38	2.85	3.55

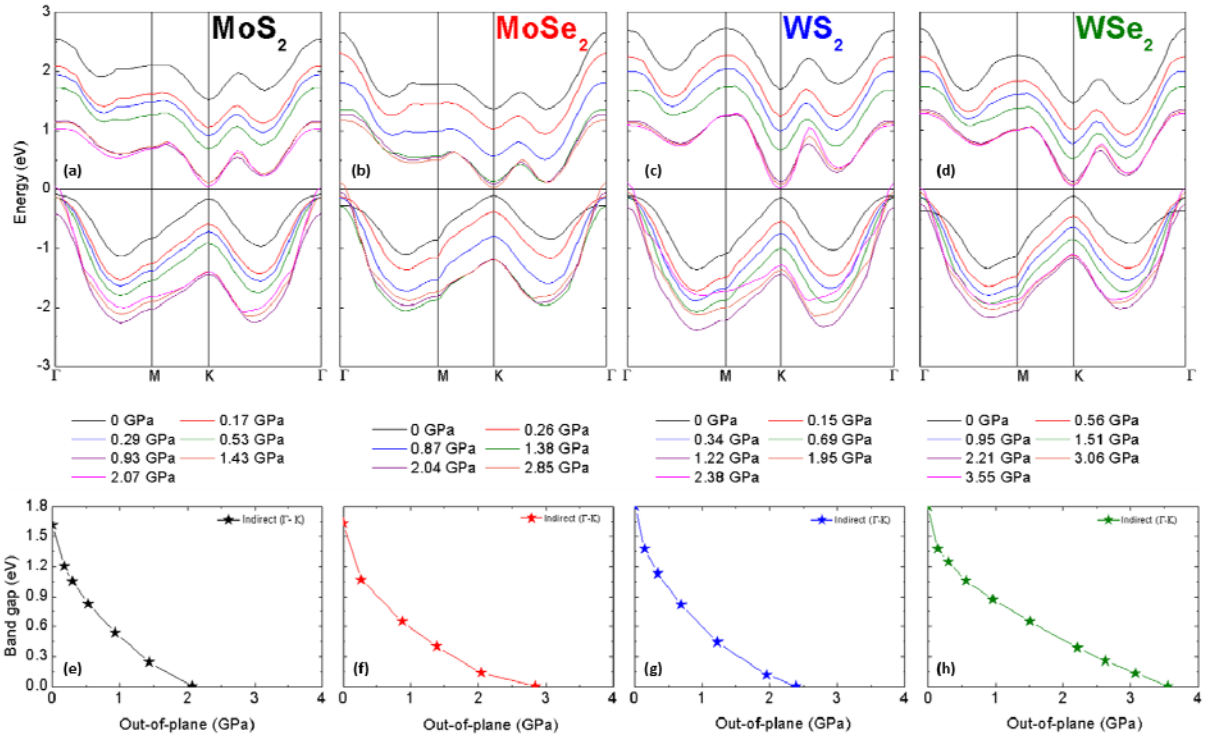

Figure 4. (a-d) Evolution of the VB and the CB bands under direct out-of-plane stress of 2L TMDs (Fermi level is set to *E*= 0 eV) at PBE level. (e-h) Evolution of the band gap (indirect) towards semimetal state under compression.

Such intriguing behavior can be explained in view of the evolution of the structural parameters with stress. In the case of 2L MX_2 we are not able to find a structural indicator of the metallization as clear as in the case of the analogous monolayers; the evolution of the structural parameters (Figure 5) is analogous for all systems; and simply, those bilayered systems with smaller bond angles and distances in the pristine state metallize at lower

pressures. In this regard, the parameters of the bilayered sulfide compounds are systematically below the selenide ones. Interestingly, among all structural parameters, the interlayer distance, labeled as $d(X\text{-}X)_{inter}$, shows the most significant changes with compression, indicating that the van der Waals space between the layers is the feature most sensitive to the effect of out-of-plane stress. Looking at Figure 5e, there is an important reduction of this parameter at the initials stages of compression (below 0.5 GPa), favoring the interaction between the orbitals [11]. This reduction is higher for sulfide systems, promoting an earlier metallization than in the selenide analogues. Hence, the changes in the electronic properties are attributed to the hybridization between out-of-plane orbitals of different layers [37] due to the effect of pressure. Following this idea, the differences of hybridization are directly related with the atomic chalcogenide radius: S^{2-} radius (184 pm) and Se^{2-} (198 pm). The bilayered compounds formed by S atoms promote a stronger hybridization of the orbitals between the layers leading to a semimetallization at lower compression, below 2.4 GPa. Under the application of direct out-of-plane pressure, the interlayer distance between the atomic planes decreases and the intra- as well as interlayer interactions alter the electronic properties of TMDs.

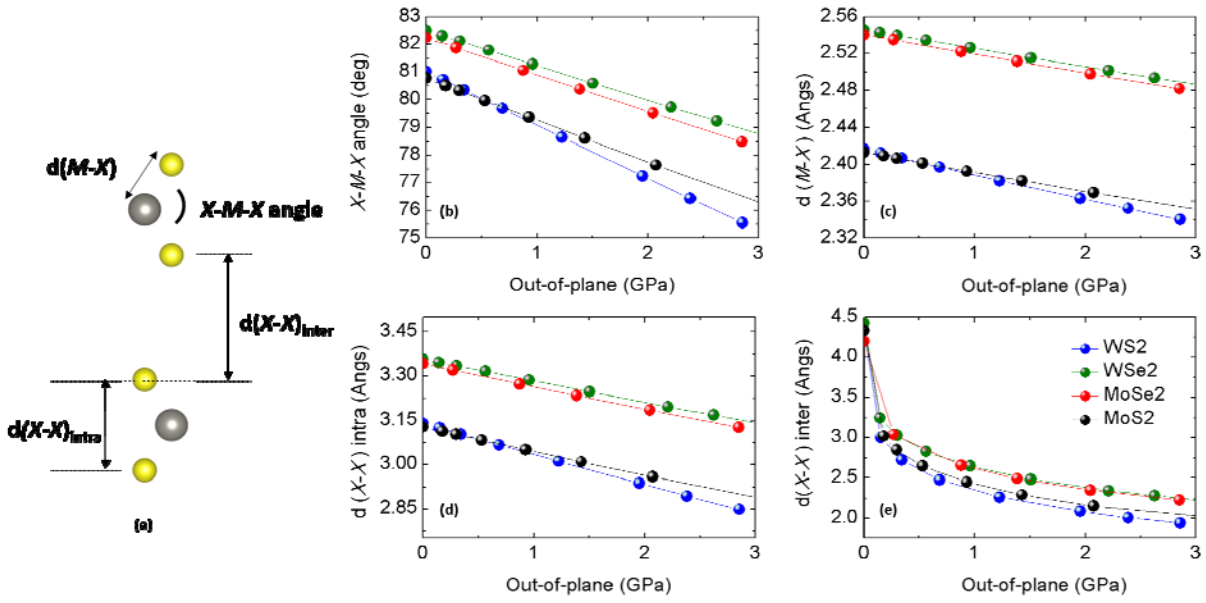

Figure 5. (a) Structural parameters of MX_2 bilayer compounds evaluated under out-of-plane compression: (b) *X-M-X* bond angle, (c) *M-X* distance, and (d) intra and (e) inter *X-X* distances.

Non-covalent domains, chemical properties

The semimetal state of mono- and bilayered MX_2 compounds is explained using the so-called non-covalent interactions (NCI) index[38-39], which is based on the reduced electron density gradient (RDG, *s*). The NCI approach has shown great success for visualizing weak interactions and enabling the characterization of both stabilizing (hydrogen bonds and vdW) and destabilizing (steric clashes) interactions in different materials[40,41]. These interactions can be highlighted within the molecular frame by means of *s* isosurfaces (Figure 6). In order to visually identify the interaction type, a color code is used [38]: blue for attractive, green for vdW and red for clashes. The NCI analysis is carried out with the CRITIC2 code [42] and the NCI domains are then visualized using VMD 1.9.1 [43]. Recently, NCI index has been used to explain the metallization of semiconductor compounds under different strain regimes [41].

This analysis has been performed for all mono- and bilayer compounds, the information obtained is qualitatively analogous to the case of MoS_2 (Figure 6). In monolayer systems (Figure 6a) the NCI domains increase in the S···S space (blue iso-surface) by the effect of strain promoting the attraction between the sulfur atoms. On the other hand, the NCI domains appear in the interlayer space of the bilayer compounds (Figure 6b). These NCI domains are not present in the pristine state and they are related with the changes of the electronic properties discussed above.

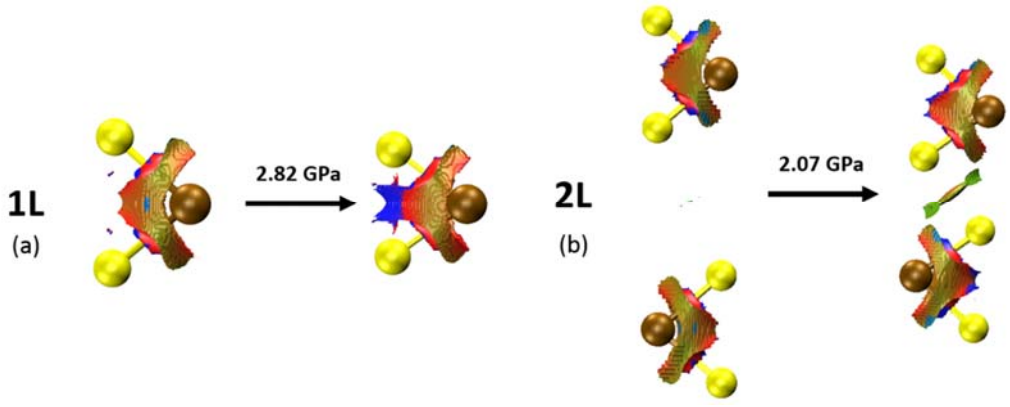

Figure 6. Domains of the reduced density gradient (RDG, *s*= 0.4 a.u.) for 1L-MoS_2 (a) and 2L-MoS_2 (b). Brown and yellow spheres correspond to Mo and S atoms, respectively.

Conclusions

The modulation of band-gap is systematically studied by means of first-principles calculations for the TMDs family: MoS_2, $MoSe_2$, WS_2 and WSe_2 (mono- and bilayer systems) under direct out-of-plane compression. This particular regime, in contrast to hydrostatic compression, reduces significantly the stress range at which the semimetal state is achieved. Two electronic transitions are reported for the monolayer systems. (i) The direct to indirect band-gap (below 1 GPa); this transition is reached in sulfides sooner than in selenides indicating a direct correlation with the chalcogenide atomic radius ($S^{2-} < Se^{2-}$). (ii) The semiconductor to semimetal transition is achieved at ~3 GPa; in this case, MoX_2 systems show lower transition stress threshold than WX_2; indicating that the hybridization of the out-of-plane orbitals is more effective in the TMDs monolayers formed by the transition metal with smaller ionic radius ($Mo^{4+} < W^{4+}$). On the other hand, the van der Waals space between the layers is the key parameter for understanding the transition to the semimetal state in bilayer systems. Here, the hybridization of the orbitals between the layers promotes the transition to the semimetal state and it is governed by the chalcogenide ion radius. Finally, the NCI index analysis confirms that the appearance of new non-covalent domains is related with the electronic changes induced by direct out-of-plane compression, reporting the consistency between the structural, electronic and chemical properties. Our predictions can be of a great utility for the experimentalist since the transition stresses reported here are easily reached using DAC devices. Our results also open plausible new ways for the synthesis of semiconductor TMDs leading to an easy modulation of the band-gap under stress.

Acknowledgements

Computational resources from Universidad de Oviedo (MALTA Supercomputing Center) provided the required computational. A. M.-G acknowledges the computer resources, technical expertise and assistance provided by the Barcelona Supercomputing Center – Centro Nacional de Supercomputación (QCM-2016-1-0019). E.d.C and O.F. acknowledge the support of the Czech Science Foundation project 14-15357S.

Uncategorized References

1. Wang, Q. H.; Kalantar-Zadeh, K.; Kis, A.; Coleman, J. N.; Strano, M. S., Electronics and optoelectronics of two-dimensional transition metal dichalcogenides. *Nat Nanotechnol* **2012,** *7* (11), 699-712.
2. Zhang, Y. J.; Ye, J. T.; Matsuhashi, Y.; Iwasa, Y., Ambipolar MoS2 Thin Flake Transistors. *Nano Lett* **2012,** *12* (3), 1136-1140.
3. Jain, J. R.; Hryciw, A.; Baer, T. M.; Miller, D. A. B.; Brongersma, M. L.; Howe, R. T., A micromachining-based technology for enhancing germanium light emission via tensile strain. *Nat Photonics* **2012,** *6* (6), 398-405.
4. Castellanos-Gomez, A.; Roldan, R.; Cappelluti, E.; Buscema, M.; Guinea, F.; van der Zant, H. S. J.; Steele, G. A., Local Strain Engineering in Atomically Thin MoS2. *Nano Lett* **2013,** *13* (11), 5361-5366.
5. Conley, H. J.; Wang, B.; Ziegler, J. I.; Haglund, R. F.; Pantelides, S. T.; Bolotin, K. I., Bandgap Engineering of Strained Monolayer and Bilayer MoS2. *Nano Lett* **2013,** *13* (8), 3626-3630.
6. Dou, X. M.; Ding, K.; Jiang, D. S.; Sun, B. Q., Tuning and Identification of Interband Transitions in Monolayer and Bilayer Molybdenum Disulfide Using Hydrostatic Pressure. *Acs Nano* **2014,** *8* (7), 7458-7464.
7. Espejo, C.; Rangel, T.; Romero, A. H.; Gonze, X.; Rignanese, G. M., Band structure tunability in MoS2 under interlayer compression: A DFT and GW study. *Phys Rev B* **2013,** *87* (24).
8. Guo, H. Y.; Lu, N.; Wang, L.; Wu, X. J.; Zeng, X. C., Tuning Electronic and Magnetic Properties of Early Transition-Metal Dichalcogenides via Tensile Strain. *Journal of Physical Chemistry C* **2014,** *118* (13), 7242-7249.
9. Peña-Alvarez, M.; del Corro, E.; Morales-Garcia, A.; Kavan, L.; Kalbac, M.; Frank, O., Single Layer Molybdenum Disulfide under Direct Out-of-Plane Compression: Low-Stress Band-Gap Engineering. *Nano Lett* **2015,** *15* (5), 3139-3146.
10. Amin, B.; Kaloni, T. P.; Schwingenschlogl, U., Strain engineering of WS2, WSe2, and WTe2. *Rsc Advances* **2014,** *4* (65), 34561-34565.
11. Nayak, A. P.; Bhattacharyya, S.; Zhu, J.; Liu, J.; Wu, X.; Pandey, T.; Jin, C. Q.; Singh, A. K.; Akinwande, D.; Lin, J. F., Pressure-induced semiconducting to metallic transition in multilayered molybdenum disulphide. *Nat Commun* **2014,** *5*.
12. Kumar, A.; Ahluwalia, P. K., Semiconductor to metal transition in bilayer transition metals dichalcogenides MX2 (M = Mo, W; X = S, Se, Te). *Model Simul Mater Sc* **2013,** *21* (6).
13. Su, X. Y.; Zhang, R. Z.; Guo, C. F.; Zheng, J. M.; Ren, Z. Y., Band engineering of dichalcogenide MX2 nanosheets (M = Mo, W and X = S, Se) by out-of-plane pressure. *Phys Lett A* **2014,** *378* (9), 745-749.
14. Nayak, A. P.; Pandey, T.; Voiry, D.; Liu, J.; Moran, S. T.; Sharma, A.; Tan, C.; Chen, C. H.; Li, L. J.; Chhowalla, M.; Lin, J. F.; Singh, A. K.; Akinwande, D., Pressure-Dependent Optical and Vibrational Properties of Mono layer Molybdenum Disulfide. *Nano Lett* **2015,** *15* (1), 346-353.
15. Zhao, Z.; Zhang, H. J.; Yuan, H. T.; Wang, S. B.; Lin, Y.; Zeng, Q. S.; Xu, G.; Liu, Z. X.; Solanki, G. K.; Patel, K. D.; Cui, Y.; Hwang, H. Y.; Mao, W. L., Pressure induced metallization with absence of structural transition in layered molybdenum diselenide. *Nat Commun* **2015,** *6*.
16. Nayak, A. P.; Yuan, Z.; Cao, B. X.; Liu, J.; Wu, J. J.; Moran, S. T.; Li, T. S.; Akinwande, D.; Jin, C. Q.; Lin, J. F., Pressure-Modulated Conductivity, Carrier Density, and Mobility of Multi layered Tungsten Disulfide. *Acs Nano* **2015,** *9* (9), 9117-9123.
17. Liu, B.; Han, Y. H.; Gao, C. X.; Ma, Y. Z.; Peng, G.; Wu, B. J.; Liu, C. L.; Wang, Y.; Hu, T. J.; Cui, X. Y.; Ren, W. B.; Li, Y.; Su, N. N.; Liu, H. W.; Zou, G. T., Pressure Induced Semiconductor-Semimetal Transition in WSe2. *Journal of Physical Chemistry C* **2010,** *114* (33), 14251-14254.

18. Wang, Y. L.; Cong, C. X.; Yang, W. H.; Shang, J. Z.; Peimyoo, N.; Chen, Y.; Kang, J. Y.; Wang, J. P.; Huang, W.; Yu, T., Strain-induced direct-indirect bandgap transition and phonon modulation in monolayer WS2. *Nano Res* **2015,** *8* (8), 2562-2572.
19. Ghosh, C. K.; Sarkar, D.; Mitra, M. K.; Chattopadhyay, K. K., Equibiaxial strain: tunable electronic structure and optical properties of bulk and monolayer MoSe2. *J Phys D Appl Phys* **2013,** *46* (39).
20. Yang, C. Z., X.; Wei S., Manipulation of electronic structure in WSe2 monolayer by strain. *Solid State Communications* **2016**.
21. Hohenberg, P.; Kohn, W., Inhomogeneous Electron Gas. *Phys Rev B* **1964,** *136* (3b), B864-+.
22. Kohn, W.; Sham, L. J., Self-Consistent Equations Including Exchange and Correlation Effects. *Phys Rev* **1965,** *140* (4a), 1133-&.
23. Kresse, G.; Furthmuller, J., Efficiency of ab-initio total energy calculations for metals and semiconductors using a plane-wave basis set. *Comp Mater Sci* **1996,** *6* (1), 15-50.
24. Kresse, G.; Furthmuller, J., Efficient iterative schemes for ab initio total-energy calculations using a plane-wave basis set. *Phys Rev B* **1996,** *54* (16), 11169-11186.
25. Perdew, J. P.; Burke, K.; Ernzerhof, M., Generalized gradient approximation made simple. *Physical Review Letters* **1996,** *77* (18), 3865-3868.
26. Blochl, P. E., Projector Augmented-Wave Method. *Phys Rev B* **1994,** *50* (24), 17953-17979.
27. Ji, J.; Zhang, A.; Xia, T.; Gao, P.; Jie, Y.; Zhang, Q.; Zhang, Q., Strain-modulated excitonic gaps in mono- and bi-layer MoSe2. *Chinese Physical B* **2016,** *25* (7), 077802(1)-077802(4).
28. del Corro, E.; Izquierdo, J. G.; Gonzalez, J.; Taravillo, M.; Baonza, V. G., 3D Raman mapping of uniaxially loaded 6H-SiC crystals. *J Raman Spectrosc* **2013,** *44* (5), 758-762.
29. Yun, W. S.; Han, S. W.; Hong, S. C.; Kim, I. G.; Lee, J. D., Thickness and strain effects on electronic structures of transition metal dichalcogenides: 2H-M X-2 semiconductors (M = Mo, W; X = S, Se, Te). *Phys Rev B* **2012,** *85* (3).
30. Wang, X. H.; Ning, J. Q.; Zheng, C. C.; Zhu, B. R.; Xie, L.; Wu, H. S.; Xu, S. J., Photoluminescence and Raman mapping characterization of WS2 monolayers prepared using top-down and bottom-up methods. *J Mater Chem C* **2015,** *3* (11), 2589-2592.
31. Tonndorf, P.; Schmidt, R.; Bottger, P.; Zhang, X.; Borner, J.; Liebig, A.; Albrecht, M.; Kloc, C.; Gordan, O.; Zahn, D. R. T.; de Vasconcellos, S. M.; Bratschitsch, R., Photoluminescence emission and Raman response of monolayer MoS2, MoSe2, and WSe2. *Opt Express* **2013,** *21* (4), 4908-4916.
32. Shannon, R. D., Revised Effective Ionic-Radii and Systematic Studies of Interatomic Distances in Halides and Chalcogenides. *Acta Crystallogr A* **1976,** *32* (Sep1), 751-767.
33. Chang, C. H.; Fan, X. F.; Lin, S. H.; Kuo, J. L., Orbital analysis of electronic structure and phonon dispersion in MoS2, MoSe2, WS2, and WSe2 monolayers under strain. *Phys Rev B* **2013,** *88* (19).
34. Chu, T.; Ilatikhameneh, H.; Klimeck, G.; Rahman, R.; Chen, Z. H., Electrically Tunable Bandgaps in Bilayer MoS2. *Nano Lett* **2015,** *15* (12), 8000-8007.
35. Jo, S.; Ubrig, N.; Berger, H.; Kuzmenko, A. B.; Morpurgo, A. F., Mono- and Bilayer WS2 Light-Emitting Transistors. *Nano Lett* **2014,** *14* (4), 2019-2025.
36. Desai, S. B.; Seol, G.; Kang, J. S.; Fang, H.; Battaglia, C.; Kapadia, R.; Ager, J. W.; Guo, J.; Javey, A., Strain-Induced Indirect to Direct Bandgap Transition in Multi layer WSe2. *Nano Lett* **2014,** *14* (8), 4592-4597.
37. Fang, S. A.; Defo, R. K.; Shirodkar, S. N.; Lieu, S.; Tritsaris, G. A.; Kaxiras, E., Ab initio tight-binding Hamiltonian for transition metal dichalcogenides. *Phys Rev B* **2015,** *92* (20).
38. Johnson, E. R.; Keinan, S.; Mori-Sanchez, P.; Contreras-Garcia, J.; Cohen, A. J.; Yang, W. T., Revealing Noncovalent Interactions. *J Am Chem Soc* **2010,** *132* (18), 6498-6506.
39. Contreras-Garcia, J.; Johnson, E. R.; Keinan, S.; Chaudret, R.; Piquemal, J. P.; Beratan, D. N.; Yang, W. T., NCIPLOT: A Program for Plotting Noncovalent Interaction Regions. *J Chem Theory Comput* **2011,** *7* (3), 625-632.

40. Christian, M. S.; Whittleton, S. R.; Otero-de-la-Roza, A.; Johnson, E. R., Chemical bonding and surface interactions in Bi2Se3 and Bi4Se3. *Comput Theor Chem* **2015,** *1053*, 238-244.
41. Guedda, H. Z.; Ouahrani, T.; Morales-Garcia, A.; Franco, R.; Salvado, M. A.; Pertierra, P.; Recio, J. M., Computer simulations of 3C-SiC under hydrostatic and non-hydrostatic stresses. *Physical Chemistry Chemical Physics* **2016,** *18* (11), 8132-8139.
42. Otero-de-la-Roza, A.; Johnson, E. R.; Contreras-Garcia, J., Revealing non-covalent interactions in solids: NCI plots revisited. *Phys Chem Chem Phys* **2012,** *14* (35), 12165-12172.
43. Humphrey, W.; Dalke, A.; Schulten, K., VMD: Visual molecular dynamics. *J Mol Graph Model* **1996,** *14* (1), 33-38.